

SANDIA REPORT

SAND2001-8366
Unlimited Release
Printed May 2001

Secondary Radiation in LIGA PMMA Resist Exposure, Part 1: The Influence of X-Ray Scattering

Aili Ting

Prepared by
Sandia National Laboratories
Albuquerque, New Mexico 87185 and Livermore, California 94550

Sandia is a multiprogram laboratory operated by Sandia Corporation,
a Lockheed Martin Company, for the United States Department of
Energy under Contract DE-AC04-94AL85000.

Approved for public release; further dissemination unlimited.



Sandia National Laboratories

Issued by Sandia National Laboratories, operated for the United States Department of Energy by Sandia Corporation.

NOTICE: This report was prepared as an account of work sponsored by an agency of the United States Government. Neither the United States Government, nor any agency thereof, nor any of their employees, nor any of their contractors, subcontractors, or their employees, make any warranty, express or implied, or assume any legal liability or responsibility for the accuracy, completeness, or usefulness of any information, apparatus, product, or process disclosed, or represent that its use would not infringe privately owned rights. Reference herein to any specific commercial product, process, or service by trade name, trademark, manufacturer, or otherwise, does not necessarily constitute or imply its endorsement, recommendation, or favoring by the United States Government, any agency thereof, or any of their contractors or subcontractors. The views and opinions expressed herein do not necessarily state or reflect those of the United States Government, any agency thereof, or any of their contractors.

Printed in the United States of America. This report has been reproduced directly from the best available copy.

Available to DOE and DOE contractors from
U.S. Department of Energy
Office of Scientific and Technical Information
P.O. Box 62
Oak Ridge, TN 37831

Telephone: (865)576-8401
Facsimile: (865)576-5728
E-Mail: reports@adonis.osti.gov
Online ordering: <http://www.doe.gov/bridge>

Available to the public from
U.S. Department of Commerce
National Technical Information Service
5285 Port Royal Rd
Springfield, VA 22161

Telephone: (800)553-6847
Facsimile: (703)605-6900
E-Mail: orders@ntis.fedworld.gov
Online order: <http://www.ntis.gov/ordering.htm>



Secondary Radiation in LIGA PMMA Resist Exposures, Part 1: The Influence of X-Ray Scattering

Aili Ting
Sandia National Laboratories
Livermore, California 94551-0969

ABSTRACT

X-ray scattering and x-ray fluorescence are two important sources of secondary radiation superposed on the primary x rays used in PMMA resist exposures for the LIGA process. The present work explores both of these sources and their impact on exposure accuracy. In particular, resist doses due to secondary radiation in the shadow region behind the mask are computed, and the potential effect of these doses on the structural accuracy of the developed PMMA is discussed.

Part 1 of this report examines the role of x-ray cross section and energy loss in Compton scattering, defines integrated energy-shift-average angles, establishes a two-layer frontscattering and backscattering model, and presents several examples illustrating the role of the resist substrate in increasing PMMA bottom-surface doses by secondary radiation. The examples given are for the NSLS synchrotron source and standard filter set. These results show that although Compton scattering plays an important role in exposure, backscattered radiation absorbed at the PMMA resist bottom surface is less than 3% of that due to direct radiation for several substrates of interest. The resulting maximum dose in the resist shadow region is about 200 J/cm^3 for normal exposure conditions.

Part 2 investigates absorption edges and transitions, shell vacancy probability, fluorescence transition and Auger transition probability, transition photon energies, and the absorbed doses associated with fluorescence x rays. Sample calculations are presented for the NSLS and SSRL synchrotron sources, the standard filter set, and several mask membrane and resist substrate materials of interest. The results show that fluorescence x rays emitted from the mask membrane and from the resist substrate may or may not lead to significant shadow-region doses, depending on the mask membrane and substrate material used and the power spectrum of the incident x rays at the material. A mid-high-Z mask membrane or resist substrate material like titanium, nickel, or copper emits fluorescence x rays that can reach the resist shadow region, leading to absorbed doses as high as $0.3\text{--}2.1 \text{ kJ/cm}^3$. With the much weaker ALS synchrotron source, however, a mid-high-Z mask membrane or resist substrate material will not emit any meaningful fluorescence x rays.

ACKNOWLEDGMENTS

The present work was funded by the LIGA project in the Sandia Revolution in Engineering and Manufacturing (REM) Program. Sandia is a multiprogram laboratory operated by Sandia Corporation, a Lockheed Martin Company, for the United States Department of Energy under contract DE-AC04-94AL85000.

The author would like to thank Stewart K. Griffiths of Sandia National Laboratories for his insightful discussion and suggestions. The author is also indebted to Stewart K. Griffiths, Dale Boehme, and Mark Perra for reading the manuscript and offering some helpful suggestions, and to Wendy Rule for her help in the editing of the manuscript.

CONTENTS

Introduction to Parts 1 and 2	6
Part 1: The Influence of X-Ray Scattering in LIGA Resist Exposures	11
Background	11
X-Ray Attenuation	12
Photon Interaction Cross Sections	14
Energy Loss in Compton Scattering	21
Two-Layer Scattering Model and Example Calculations	26
Conclusion of Part 1	34
References	35
Appendix: Basic Interactions Between Photons and Atoms	38

Figures

1. Power Spectrum Switches by Filter Set in SSRL Synchrotron Source	14
2. Normalized Power Spectrum Switches by SSRL Standard Filters	14
3. Cross Sections for Si	16
4. PMMA Cross Sections	16
5. Energy Loss Due to Compton Scattering on PMMA Top Surface After Standard Filter Sets	17
6. Power Spectrum Output From Four Light Sources	17
7. Absorption Cross-Section Spectra of Materials	18
8. X-Ray Attenuation in Al	20
9. Dimensionless Absorption Factor Modeled by LEX-D and PHOTON	20
10. Wavelength Change After Compton Scattering	22
11. Compton Photon Energy vs. Scattering Angle	22
12. Average Energy Loss in Compton Scattering	24
13. K-N Compton Collision Cross Section per Unit Solid Angle	25
14. Ratios of Backscattering Cross Section to Frontscattering Cross Section From Klein-Nishina Equation	25
15. K-N Collision Cross Section vs. Scattering Angle	26
16. Average Energy Degradation by Compton Scattering	26
17. Average Backscattered Power Fluxes for NSLS Example	31
18. Average Backscattered Dose Rate for NSLS Example	31

Table

Scattering Results for NSLS Standard Filter Set + Resist + Substrate

30

INTRODUCTION TO PARTS 1 AND 2

X-ray exposure and PMMA—poly(methyl methacrylate)—resist development are two important steps in the LIGA process that together largely determine the precision and tolerances of finished parts.^[1-5] The acronym LIGA comes from the German words for lithography, electroplating, and molding. During a LIGA exposure, incident x rays from a synchrotron source pass through a series of filters and an absorber mask to pattern the PMMA resist. Absorption of radiation energy in the exposed portions of the resist leads to main-chain molecular scissions of the polymer, producing a short-chain polymer of reduced molecular weight. Cross-linking reactions may also result, though these are generally of secondary concern for the PMMA. Exposed portions of the resist thus become soluble in organic solvents. Development of the resist in such solvents then produces a PMMA microstructure that can be used as a finished part or can serve as a mold for electroforming metal devices.

The quality of the microstructure produced by LIGA depends strongly on both the exposure and development steps. A good exposure must produce an acceptable distribution of the dose through thick resists but must also provide high dose contrast between the masked and unmasked regions. Development times for thick resists may run from a few hours to a day or more, depending on feature aspect ratios. For that reason, even fairly small doses in masked regions may yield lateral development rates high enough that overall development of feature sidewalls is significant.^[6-8] Limiting the absorbed dose in the shadow region thus plays an important role in ensuring small tolerances both on lateral feature dimensions and on the vertical taper of feature sidewalls. Because secondary radiation can contribute significantly to total doses in the shadow region, some understanding of the sources of this radiation and its transport and absorption in the resist is required.

In order to have complete development at reasonable development rates, the bottom-surface dose of a PMMA resist must exceed some minimum value, around 3 or 4 kJ/cm³. The top-surface dose thus depends on the thickness of the resist, the incident x-ray spectrum, and the required bottom dose. It is also required that the top-surface dose be below some maximum value to avoid developing bubbles from noncondensable gases formed by excessive x-ray fluxes. These competing requirements are met through the use of a combination of beam filters appropriate to the x-ray source and an appropriate exposure time. The dose throughout the resist in the shadow region should be sufficiently small that sidewall development is acceptably small over the course of development. The value of this dose, typically below 1 kJ/cm³, depends on the initial state of the PMMA

resist (molecular weight and degree of cross-linking) and on properties of the developer solvent.

Beyond their influence on tolerances, absorbed doses in the shadow region may also contribute to undercutting of features at the interface between the PMMA and the substrate to which it is bonded. If the absorbed resist dose in the shadow region is excessive, the developer will attack the bond layer at the interface once a feature is fully developed. This can lead to the detachment of desired features such as columns and webs, which are then washed away by developer.^[9] This makes it difficult to produce high-aspect-ratio gear shafts and locator posts by current LIGA practices. Again, secondary radiation may contribute to the total dose in the shadow region near the interface between the resist and substrate, and so may contribute to undercutting. Understanding the development process associated with low absorbed doses is also essential to controlling undercutting and feature detachment. Low-dose development rates will be addressed in a future study.

For exposed PMMA developed in GG developer^[1]—60% 2-(2-butoxyethoxy) ethanol, 20% morpholine, 5% ethanolamine, and 15% de-ionized water—or other, similar, solvents, the minimum bottom-surface dose to obtain reasonable development rates and total development times is roughly 4 kJ/cm^3 ,^[9,10] and the maximum top-surface dose to avoid bubble formation is about 15 to 20 kJ/cm^3 . The maximum tolerable dose in the shadow region is reported by different sources as about 100 J/cm^3 ,^[9] 1.5 kJ/cm^3 ,^[10] or 1.8 kJ/cm^3 .^[11,12] Obviously there is wide variation in reported values of the acceptable dose, and experiments are needed to help resolve the discrepancies. Experience within the Sandia/California LIGA group suggests that 1.5 and 1.8 kJ/cm^3 are probably too high.

Among all possible factors in exposure physics likely to produce large shadow-region doses over large ranges, x-ray scattering and fluorescence x rays are dominant. Photoelectrons are also known to produce very large doses, but their range is extremely small. When photons from the primary x rays encounter the loosely bound electrons in outer shells of a material, the photons change direction by scattering, with an associated loss of energy (see the appendix to Part 1). Scattering in the PMMA may thus redirect incoming photons passing through open regions of the mask toward the shadow region at the resist bottom surface. However, these scattered x rays can be absorbed as they continue toward the resist bottom surface. They may also be scattered in a direction that does not intersect the bottom surface. Similarly, x rays passing through mask openings and through the PMMA may be scattered backward from the resist substrate body and subsequently absorbed in resist shadow regions near the substrate. Thus primary x rays scattered by both the PMMA and the PMMA substrate may contribute to the absorbed dose in resist shadow regions near the substrate.

Fluorescence x rays are produced when a primary x-ray photon with enough energy is absorbed. The resulting fluorescence x ray has a lower energy than the primary x ray that produced it. When this occurs at the PMMA substrate, the fluorescence x ray may travel backward toward the bottom surface of the resist and, if absorbed, may also contribute to the total dose in the shadow region. Likewise, fluorescence x rays can be created at the mask membrane, and these can possibly reach the shadow region at the resist top surface.

Although all secondary photons are of lower energy than the primary radiation, they may still pass through much of the PMMA thickness and can be absorbed in shadow regions near the substrate. However, most of this secondary radiation from the mask membrane and resist substrate will be absorbed somewhat near its source. Secondary radiation is thus likely to be most important at the resist top and bottom surfaces and near feature boundaries, especially corners, where secondary radiation may arrive from several different directions.

In 1985 Murata^[13] investigated monochromatic x-ray scattering at a resist-substrate interface using Monte Carlo simulation. The x-ray line was the aluminum (Al) K-shell fluorescence line with an energy of 1487 eV and a wavelength of 0.834 nm, and the target was a 1.0- μm PMMA resist on a silicon (Si) substrate. This configuration can be viewed either as primary monochromatic x rays scattering at the interface or as fluorescence x rays generated by an Al filter placed above the resist and interacting with the interface. Murata concluded that scattered radiation penetrated about 0.02–0.035 μm into the resist shadow region, and that photoelectrons escaping from the interface penetrated only about 0.015 μm . The areal energy density in this study was about 10^{-9} J/cm². However, the resist thickness was far too thin to be of direct interest for LIGA. Also, the x-ray line energy was not strong— in the range of soft x rays.

Pantenburg and Mohr^[9] at KfK (Kernforschungszentrum Karlsruhe, the Institute of Micro-structure Technique) studied the effects of secondary radiation by fluorescence x rays and photoelectrons on LIGA structures in 1995. For secondary radiation from a 2- μm resist substrate to a 100- μm resist, they found that the adhesion of the developed resist structures was greater for a carbon (C) substrate than for a titanium (Ti) substrate, unless the gold (Au) absorber thickness was increased for the latter. This is because Ti produces much harder fluorescence photons than those generated by C. Increasing the Au thickness simply reduces primary x-ray penetration to the substrate to create fluorescence. For secondary radiation from a Ti mask membrane to a 1000- μm resist, they found visible distortion of the structure edge after development beyond 200 μm . Placing a preabsorber between the mask and the resist to absorb fluorescence, or using a mask membrane with a low atomic number (Z), such as beryllium (Be), Si, or diamond, greatly reduced the

distortion. No known simulations have verified the 200- μm penetration into the resist shadow region, which Pantenburg and Mohr claimed was due to K fluorescence x rays emitted by the Ti mask membrane.

In 1996 Schmidt et al.,^[14] with the well-known German group led by W. Ehrfeld, investigated the adhesive strength of PMMA structures on substrates under synchrotron radiation. They performed Monte Carlo simulations for a 500- μm PMMA resist paired with substrates such as Ti, copper (Cu), and glassy carbon. They also measured the bond strength at the PMMA and substrate interface. Their results show that for higher- Z substrates like Cu and Ti, PMMA columns break at a lower tension and that the bond-breaking tension for glassy carbon substrates was about twice as high as that for Ti substrates at the same dose. Their results showed 0.3 and 0.75 μm depths of development into the resist shadow region for Ti and Cu substrates, respectively, but no similar undercutting for glassy carbon substrates. They believed that this was due to escaping photoelectrons and Auger electrons (see the appendix to Part 1, and Part 2), and that fluorescence x rays generated by Ti and Cu substrates were not important.

In 1997, using Monte Carlo simulation, Zumaque et al.^[10] investigated secondary radiation, including fluorescence x rays, escaping photoelectrons, and Auger electrons. All of these may degrade the developed structure. Their analysis addressed lateral motion of electrons at the shadow-region boundary, backscattering from the resist-substrate interface, and frontscattering from the resist top surface. They found that these various sources lead to significant shadow-region doses only within submicron regions of the fully-exposed PMMA. They thus concluded that there is no evidence for micron-scale degradation of the developed patterns, as observed in the results of Pantenburg and Mohr,^[9] and that the main limiting factor in obtaining more stringent tolerances is poor understanding of the chemical processes that occur during development. Because of the limitation of their computer capacity, the number of photons used in their study was only about 2.5×10^8 , so their resist top-surface dose was only about 1.5 kJ/cm^3 . This is very much lower than typical LIGA exposure requirements, and it is probably not appropriate to extrapolate the results of Zumaque et al. to the cases of normal exposure conditions.

Also in 1997, Feiertag et al.,^[11,12] of the same German group led by W. Ehrfeld, used Monte Carlo simulations to conclude that photoelectrons cause image blur in LIGA structures and that fluorescence radiation does contribute to dose deposition in the resist if the mask membrane and resist substrate are high- Z materials. They also concluded that scattered radiation is negligible ($100\text{--}120 \text{ J/cm}^3$ in the resist shadow region) if the resist thickness is less than a few millimeters. They claim that beam divergence and Fresnel diffraction are both less important still. For a 500- μm -thick PMMA resist, their results indicate that photoelectrons yield an excess absorbed dose of 1.8 kJ/cm^3 extending into

the resist shadow region about $0.4 \mu\text{m}$ at the resist top surface and about $0.2 \mu\text{m}$ at the resist bottom surface. Their results for fluorescence x rays, presented in a figure, indicate that a 500 J/cm^3 excess absorbed dose will result in the shadow region at the resist bottom surface when a Ti resist substrate is employed. They further infer that a comparable excess dose will be deposited at the resist top surface by fluorescence radiation from a Ti mask membrane. In their second paper,^[12] however, the same figure is explained as the resist top-surface dose due to a Ti mask membrane. It is not clear which one is the true result. They also state without support in the first and second papers, respectively, that the overall fluorescence dose for a Cu substrate is eight times smaller and two times smaller than that for a Ti substrate. The reason for the difference is probably that the upper bound of the photon energy range they used is only 10 keV. The K-shell binding energy for Cu is about 8.9 keV, while that for Ti is about 4.9 keV; many fewer photons from the spectrum they used are available to excite a Cu K-shell transition than are available to excite the same transition in Ti. In addition, their post-development measurements indicate that the 1.8 kJ/cm^3 threshold profile in the resist is curved, which they ascribe to photoelectrons and fluorescence by high-Z membrane and substrate materials.

From the above previous work, we see that no consistent conclusions have been reached regarding the importance of secondary radiation in LIGA exposures either by x-ray scattering or by fluorescence x rays. Even within the single German group, one paper^[11] concludes that fluorescence x rays yield significant excess doses in the shadow region while scattered x rays do not. Just the opposite is stated in another paper^[14] by members of the same group. Further investigation is clearly needed. In this present work, excess doses in the resist shadow region are computed and discussed. The contributions from x-ray scattering and backscattering and from fluorescence x rays are studied separately in Part 1 and Part 2 of this report, respectively. In each part, each type of secondary radiation is examined from the perspectives of its origins, its transport characteristics, and its total influence on the absorbed shadow-region dose. Development is not considered in these two studies.

PART 1: THE INFLUENCE OF X-RAY SCATTERING IN LIGA RESIST EXPOSURES

BACKGROUND

During a LIGA x-ray exposure, incident x rays from a synchrotron source pass through a series of filters and a masked polymer resist (PMMA) and a resist substrate. The exposed resist in its unmasked region absorbs the radiation energy and thus becomes soluble in an organic developer because its molecules undergo a change in chemical structure. It is then shaped into a three-dimensional microscopic image, or microstructure, according to the mask pattern through the LIGA development process.^[1] This PMMA microstructure can be a product itself or can serve as a mold for electroforming metal devices.

The quality of the microstructure produced depends on both the exposure and development stages. Only exposure is discussed in this work. The goal in exposure is to ensure a desirable dose distribution in the unmasked region of the resist, and to limit any unwanted dose in the masked region, in order to generate a designed feature shape in the development process. After hours of development time, a small masked region that has received even a low dose of radiation can become distorted and damaged. If this occurs at the interface between the resist and its substrate, it can contribute to undercutting of small features and even washing away of slender feature columns of the microstructure. Therefore, understanding x-ray exposure physics—especially x-ray attenuation in a medium (including transmission and absorption) and x-ray scattering, particularly incoherent (Compton) scattering—will be the center of discussion. Although scattering is only a secondary source of radiation, backscattered x rays from the resist substrate may be an important contributor to resist undercutting. One of the goals of this work is to estimate the amount of backscattered x-ray energy at the resist-substrate interface.

Earlier Sandia LIGA experimental work used the CXRL code (developed by the Center for X-Ray Lithography, University of Wisconsin) from Lawrence Berkeley National Laboratory (LBNL)^[15] to estimate x-ray doses in the resist. Sandia's work combined the measurement data by tracing the positions of the moving surface of the feature shape in the resist during the development process to establish an empirical relationship between development rate and absorbed dose.^[1] The relation is important for designing and guiding future LIGA development experiments. In parallel, one of Sandia's major modeling efforts has been to develop its own LIGA exposure and development code, LEX-D.^[16] Combining x-ray exposure physics, polymer dissolution physics, and resist fragment transport, this code employs a phenomenological (rather than a reaction

chemistry) relationship between development rate and absorbed dose based on measured rates. Furthermore, by both analytical and numerical analysis, the code has been designed to optimize the exposure and development parameters with a user-friendly interface. During earlier experimental LIGA work at Sandia, some discrepancies were found between exposure calculations from the CXRL code and the PHOTON code from Brookhaven National Laboratory,^[17,18] especially for exposure to higher-energy light sources. The main reason is that no incoherent (Compton) scattering effects were included in the CXRL cross-section database,^[19,20] though Compton scattering is especially important for photon energies in the high-keV to mid-MeV range. LEX-D has included the Compton scattering effect.^[16]

Because tolerances and undercutting are drawing more and more concern, it is imperative to investigate x-ray scattering, especially backscattering. Further analysis and a two-layer model based on similar baselines of LEX-D produced sample calculations of the scattering radiation at the resist-substrate interface for several substrate materials of interest. The following sections address x-ray attenuation, photon interaction cross sections, energy loss in Compton scattering, and a two-layer scattering model. Examples of frontscattering and backscattering calculations are presented.

X-RAY ATTENUATION

According to quantum theory, x-ray beams consist of showers of photons—particles of energy without electric charge, traveling with the speed of light. On the other hand, an x-ray beam is also an electromagnetic wave, and its radiation is in the form of electromagnetic radiation. The equation $E = h\nu = hc/\lambda$ (where E is photon energy, h is Planck's constant, ν is frequency, and λ is wavelength) indicates that highly penetrating x-ray photons have high frequency and short wavelength, whereas weakly penetrating x-ray photons have low frequency and long wavelength.

When x rays travel into a medium, the flux attenuates because of interactions between photons and the atoms of the medium along the beam path. These interactions give rise to absorption of the radiation by the medium and to the emission of secondary radiation, including scattered radiation, those x-ray photons changing direction after interacting with atoms, and also fluorescence radiation, the characteristic radiation emitted by atoms after having absorbed x-ray photons.

Five types of basic interaction may occur between the photons and atoms along the beam path: photoelectric interaction, coherent scattering, incoherent scattering (Compton

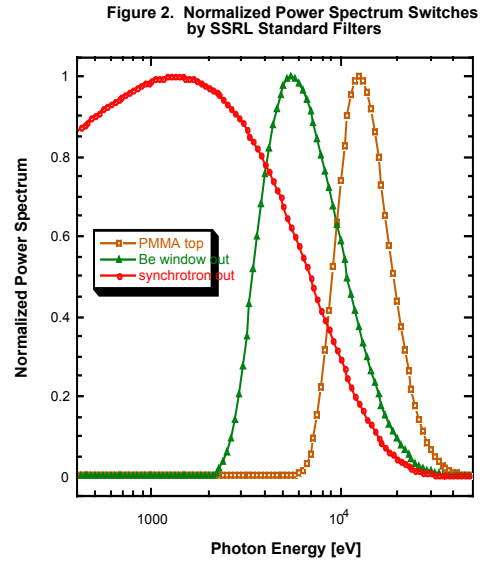
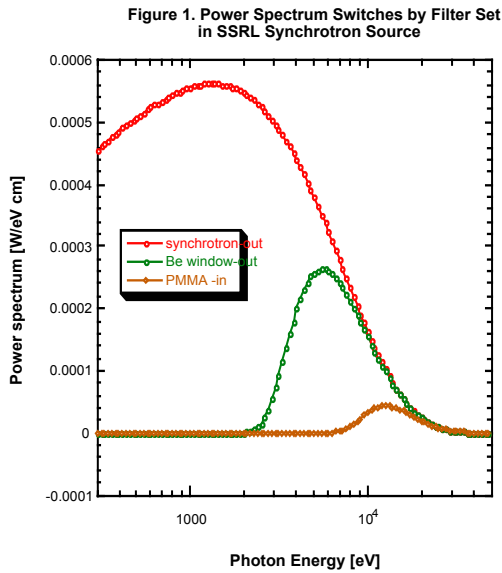
scattering), pair production, and triplet production. A brief description of how these interactions contribute to x-ray attenuation is presented in the appendix.

In the LIGA process, photon energies never reach the MeV level. Pair and triplet production will therefore never occur. The production of photoelectrons, fluorescence x rays, Compton recoil electrons, and Compton scattered photons are the results of absorption of radiation by the medium. Among them, the photoelectric effect is the most important, while scattered photons and fluorescence are a less energetic, secondary effect in the photon energy range of interest (up to 50 keV). Coherent scattering does not contribute to energy deposition, since it has no energy loss. Compton scattering, however, is not negligible beyond 10 keV, and it could be a noticeable fraction of total attenuation.

To produce the optimal resist exposure, there is a minimum dose required to create sufficient structure change and a maximum dose beyond which bubbles and swelling will be created in the resist. To achieve this, hardening of an x-ray beam from a synchrotron light source by filters is usually adopted. Filters, typically made of materials with low atomic number, absorb more low-energy photons than high-energy photons, so that the x-ray spectrum after these preabsorbers is shifted to higher photon energy. In the Sandia LIGA exposure layout, a Be vacuum window is always set as a first filter separating the high-vacuum light source from the helium (He) or air atmosphere. It is chosen for its high transparency for short-wavelength photons. It is a fixture of the light source. Optional filter materials chosen by the Sandia LIGA group include Al, C, Si, and silicon nitride (SiN), along with an air layer or He layer. PMMA is used as the resist; it is adhered to a substrate. Optional materials for the resist substrate include Si, Ti, Be, C, nickel (Ni), Cu, and stainless steel (18% Ni, 8% chromium, or Cr, and 74% iron, or Fe). A mask set—a mask absorber, usually Au, and a mask membrane (mask substrate)—is positioned before the resist. Optional materials for the mask membrane include Si, Ti, and other materials. Gas layers are maintained between the filter set, the mask set, and the resist, mainly to prevent the high-temperature heat flux coming from the light source from damaging the sample. Inert gas, such as He, is used to prevent corrosion.

Figure 1 is an example of the power spectra calculated by LEX-D using the standard filter set of the SSRL (Stanford Radiation Laboratory at Stanford University) synchrotron light source. The three curves here represent the power spectrum from the light source, after the Be window, and on the top surface of the PMMA sample, respectively. Figure 2 shows normalized power spectra of these three curves. The standard filter set used here is in the following order: Be (533 μm), He (10,000,000 μm), C (15.2 μm), Al (35 μm), air (150,000 μm), Al (110 μm), and sample resist PMMA (1100 μm). In Figure 1, the peak values of power from the synchrotron, after the Be window, and before the PMMA are $5.62e^{-4}$, $2.64e^{-4}$, and $4.358e^{-5}$ W/eV, respectively, corresponding to photon energy of

1.38, 5.495, and 12.589 keV, respectively. The power peak decays with each filter and shifts to the higher photon energy range or shorter wavelength because of absorption of low-energy photons. This is easier to identify in Figure 1. The total shift in photon energy for the power peak is about 11.21 keV from the synchrotron output to the PMMA. Therefore Compton scattering can certainly be said to play a significant role in PMMA exposure at its photon energy range here, and that role is not negligible.



PHOTON INTERACTION CROSS SECTIONS

The linear attenuation coefficient μ for a medium in an x-ray exposure is related to the penetration length λ_1 (or attenuation length, extinction length, total mean free path) as $\mu = 1/\lambda_1$. A mass attenuation coefficient is related to the linear attenuation coefficient as $\sigma = \mu/\rho = 1/(\lambda_1\rho)$, where ρ is the density. This is the cross section, related directly to the probability of collision between photons and atoms. Unlike the linear attenuation coefficient, the mass attenuation coefficient (or mass attenuation cross section) is independent of density and phase; therefore it is a more appropriate and useful quantity for describing the decay of x-ray energy in a medium.

The total mass attenuation cross section can be written as the sum of contributions from the principal photon interactions

$$\sigma_{\text{tot}} = \sigma_{\text{pe}} + \sigma_{\text{coh}} + \sigma_{\text{incoh}} + \sigma_{\text{pair}} + \sigma_{\text{trip}}$$

where σ_{pe} is the photoelectron cross section, σ_{coh} and σ_{incoh} are the coherent and the incoherent (Compton) scattering cross sections, respectively, and σ_{pair} and σ_{trip} are the cross sections for pair and triplet production, respectively. Each cross section is wavelength dependent and hence is a function of photon energy E for a particular medium.

The mass energy-absorption coefficient, or cross section σ_{abs} , can be written as

$$\sigma_{\text{abs}} = \sigma_{\text{peabs}} + \sigma_{\text{incohabs}} + \sigma_{\text{pairabs}} + \sigma_{\text{tripabs}}$$

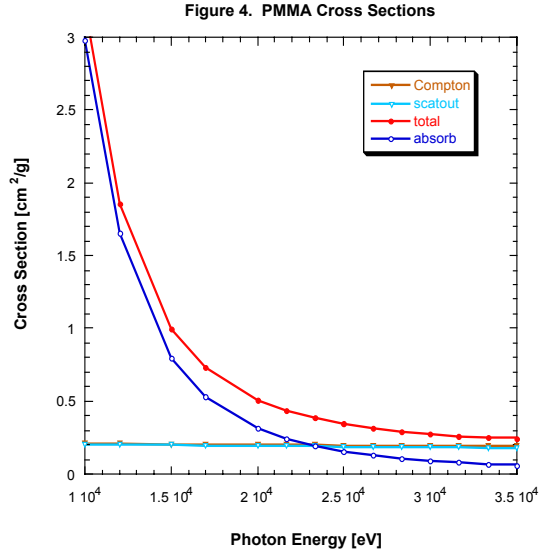
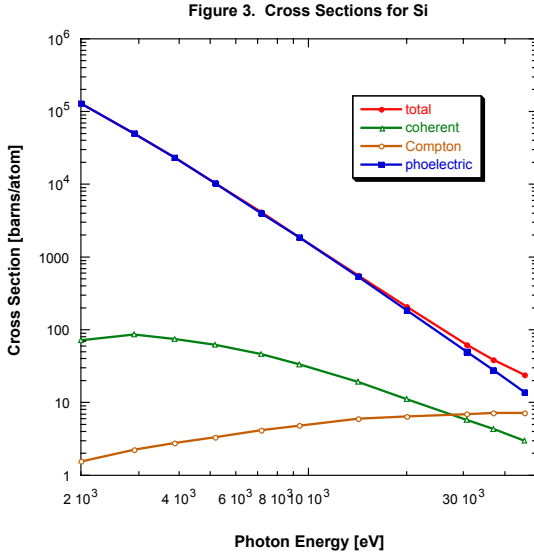
where σ_{peabs} is the photoelectric absorption cross section excluding the radiative losses for the photoelectrons, σ_{incohabs} is the energy deposition cross section due to incoherent scattering, and σ_{pairabs} and σ_{tripabs} are energy deposition cross sections due to pair and triplet production, respectively. Again, each cross section is a function of wavelength or photon energy E for a particular medium. Coherent scattering does not contribute to energy absorption.

The photon-atom interaction cross sections for a material are functions of the atomic number, Z , of that element. The cross section for a composite material is calculated from a weighted sum of the corresponding cross sections of the elements, using mass fraction as the weighting factor.

Figure 3 shows Si cross sections of σ_{tot} , σ_{pe} , σ_{coh} , and σ_{incoh} . Data are from the Lawrence Livermore National Laboratory (LLNL) Evaluated Photon Data Library, or EPDL.^[21] The unit here is barns/atom; it can be converted to cm^2/g by the factor $N_0 / (A \times 10^{24})$, where N_0 is Avogadro's number and A is atomic weight based on $^{12}\text{C} = 12$. For Si the total cross section is nearly the same as the photoelectric cross section except at photon energy greater than 30 keV, where the coherent and—especially—incoherent scattering cross sections cease to be negligible.

Figure 4 shows PMMA cross sections of σ_{tot} , σ_{abs} , σ_{incoh} and $\sigma_{\text{tot}} - \sigma_{\text{abs}} = \sigma_{\text{scatout}}$ from the Biggs and Lighthill database.^[22–24] The difference between the total cross section and the energy deposition cross section is significant only beyond 10 keV. The Compton cross section and scattering loss are hard to distinguish. If only a very small amount of Compton scattering x-ray energy is being absorbed by the PMMA, most of it will be loss. At 10 keV, the Compton scattering cross section is about 10% of the total cross section; beyond 20 keV, it is on the same order as the total cross section. Therefore, because x-ray

energy reaches the PMMA mostly in the high photon energy range, the Compton effect plays an important role and cannot be ignored.

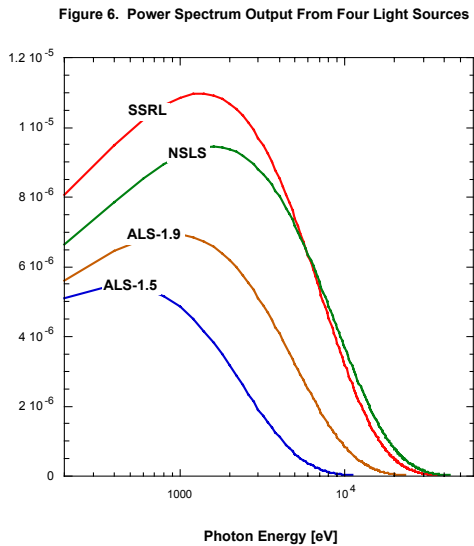
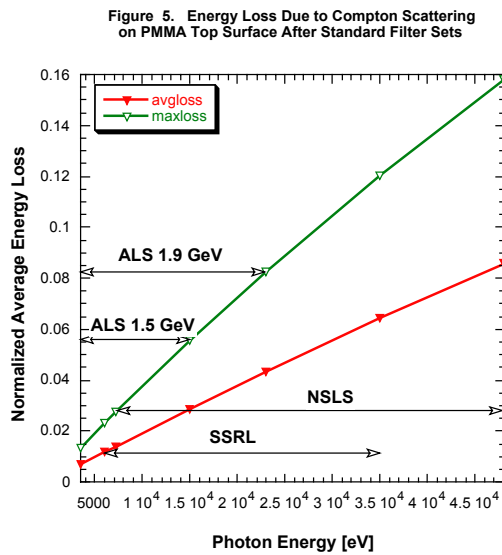


The cross-section databases from the different sources referenced in this document are good resources to consult for detailed information on cross sections. Earlier Sandia used the CXRL database^[19,20] to calculate x-ray exposure in its LIGA sample. This database includes coherent scattering but does not include Compton scattering for the photon energy range up to 30 keV. It indicates that attenuation of radiation energy is caused solely by absorption, not by any energy loss ($\sigma_{\text{tot}} = \sigma_{\text{abs}}$). For a less strong synchrotron light source (the ALS, or Advanced Light Source, at LBNL) running in both 1.9-GeV and 1.5-GeV modes with maximum beam current of 200 mA and 400 mA, respectively, the errors in absorbed doses on filters and sample are noticeable at photon energy close to 30 keV for 1.9-GeV runs but still can be tolerated. However, for much stronger synchrotron light sources (SSRL and NSLS, the National Synchrotron Light Source at Brookhaven National Laboratory) running at 3.0 GeV and 2.6 GeV with maximum beam current of 100 mA and 300 mA, respectively, the errors in energy flux and absorbed doses become intolerable because Compton scattering, which becomes important in the middle photon energy range, is not accounted for.

Figure 5 shows the normalized energy loss due to Compton scattering on the PMMA top surface after standard filter sets for all four synchrotron sources. The loss increases with photon energy almost linearly. Here the photon energy range for each source covers the significant part of the source's power spectrum. The average and maximum energy loss due to the Compton effect could be up to about 3%, 4.3%, 6.3%, or 8.6% and 5.5%, 8.25%, 12%, or 16% for photon energy up to 48 keV for light sources ALS 1.5 GeV, ALS

1.9 GeV, SSRL, and NLS, respectively. Clearly, improving the cross-section database is necessary.

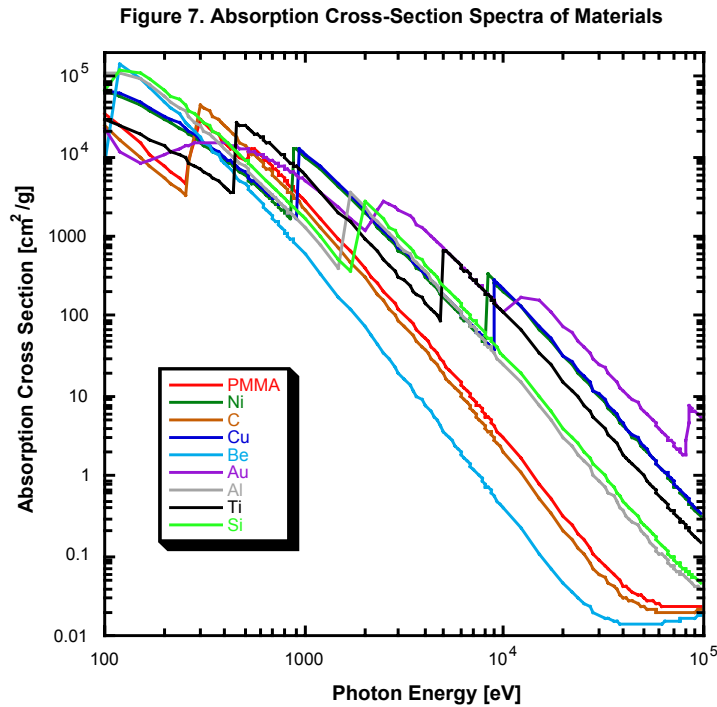
Figure 6 shows the power spectrum from each of the four synchrotron light sources. Apparently, power outputs—expressed as watts per milliamp of beam current density and per millirad of horizontal scanning angle of the synchrotron—from the NLS and SSRL sources are much stronger than the output from the ALS source running in either mode. Below 6 keV, the SSRL output is stronger than the NLS, but beyond 6 keV, the NLS output is stronger than the SSRL. The upper bound of photon energy is the highest for the NLS source, followed by the SSRL source, the ALS 1.9 GeV source, and the ALS 1.5 GeV source.



Sandia’s investigation of available databases compares LLNL’s EPDL database,^[21] the NIST (National Institute of Standards and Technology) database,^[25] the database used by the Brookhaven NLS software PHOTON,^[17,18] and the Biggs and Lighthill database.^[22–24] These databases all include Compton scattering and agree with each other well over the photon energy range of interest but disagree with the CXRL database starting from 7 keV for light elements ($Z < 10$) and starting from 10 keV for most other media of interest. The errors increase with increasing photon energy. As an example, for the LIGA PMMA resist material, the CXRL total cross section is about $0.032 \text{ cm}^2/\text{g}$, while all other databases predict about $0.23 \text{ cm}^2/\text{g}$ at photon energy 30 keV. The Sandia work has adopted a new database based on Biggs and Lighthill that is sufficient to our needs and includes Compton scattering up to the higher energy range (up to 100 keV). The Biggs and Lighthill database was chosen in preference to the EPDL, which is probably considered more sophisticated in that it extends to a very wide photon energy range (10 eV–100 GeV) and includes some new developments of recent years, mostly at

the MeV photon energy level; these new developments are beyond the energy range used in LIGA applications. The reason NIST was not chosen is that the lowest photon energy level represented in its database is 1 keV; energies below this are also of interest in LIGA.

With the new cross-section database, the exposure calculation from a single attenuation coefficient database (CXRL) is modified to include two separate attenuated cross-section databases σ_{tot} and σ_{abs} (Biggs and Lighthill^[22-24]). Figure 7 shows the total mass absorption cross section σ_{abs} for the materials typically chosen as filter, mask absorber, mask membrane, resist, and resist substrate: Be, C, Al, Si, Ti, Ni, Cu, Au, and PMMA. All absorption cross-section curves indicate a decreasing trend with photon energy, E , and an increasing trend with the atomic number, Z , of the material. More specifically, on the basis of atomic physics, they are approximately proportional to Z^4 and E^{-3} . Thus, the higher the atomic number of the material, the more x-ray absorption for a photon energy E ; the higher the photon energy, the more penetration of photons (without absorption) for a material. The zigzag shapes in the curves occur at absorption edges, where the photon energies are the same as the atomic shell binding energies of the K shell, the L shell, and so on, as photon energy decreases. Absorption occurs only when a photon energy is greater than a shell's binding energy; the cross-section curves hence jump at a photon energy just below that shell's binding energy.



In an x-ray exposure of a medium with an incident power, the radiative energy flux transmitted or penetrating a medium to a depth x , $Q_{\text{tran}}(x)$, can easily be obtained by integrating the spectral energy flux contribution, which is attenuated by the total mass attenuation cross section, over the entire spectrum of photon energy. In a similar way, the absorbed radiative energy flux of a medium at depth x , $Q_{\text{abs}}(x)$, is the integration of the fractional loss of the transmitted energy flux over the entire spectrum of photon energy. The fraction here is the absorption cross section over the total attenuation cross section, $\sigma_{\text{abs}}(E) / \sigma_{\text{tot}}(E)$. The real energy loss, $Q_{\text{scatout}}(x)$, results from scattering and hence is the difference between the total loss of energy flux in the transmission and the absorbed energy flux. The dose rate of the x-ray absorption at depth x , $D_{\text{abs}}(x)$, then, is the derivative of the absorption energy flux with respect to x . It is thus just the integration of the transmitted energy flux divided by the absorption length, $(\sigma_{\text{abs}} \rho)^{-1}$, over the entire spectrum of photon energy. The expressions for these relationships are

$$Q_{\text{tran}}(x) = \int_0^{\infty} I(\varepsilon, x_1) \exp[-\sigma_{\text{tot}}(\varepsilon)(x - x_1)\rho] d\varepsilon$$

$$Q_{\text{abs}}(x) = \int_0^{\infty} I(\varepsilon, x_1) \{1 - \exp[-\sigma_{\text{tot}}(\varepsilon)(x - x_1)\rho]\} \frac{\sigma_{\text{abs}}(\varepsilon)}{\sigma_{\text{tot}}(\varepsilon)} d\varepsilon$$

$$Q_{\text{scatout}}(x) = \int_0^{\infty} I(\varepsilon, x_1) \{1 - \exp[-\sigma_{\text{tot}}(\varepsilon)(x - x_1)\rho]\} \frac{\sigma_{\text{tot}}(\varepsilon) - \sigma_{\text{abs}}(\varepsilon)}{\sigma_{\text{tot}}(\varepsilon)} d\varepsilon$$

$$D_{\text{abs}}(x) = \frac{dQ_{\text{abs}}(x)}{dx}$$

$$D_{\text{abs}}(x) = \int_0^{\infty} I(\varepsilon, x_1) \exp[-\sigma_{\text{tot}}(\varepsilon)(x - x_1)\rho] \sigma_{\text{abs}}(\varepsilon) \rho d\varepsilon$$

where x is along the beam line direction, x_1 is the top surface of the layer, $I(\varepsilon, x_1)$ is the incident intensity at the top surface, and ρ is the medium density. All of the calculations here include Compton scattering effects in $\sigma_{\text{tot}}(\varepsilon)$ and $\sigma_{\text{abs}}(\varepsilon)$.

Figure 8 shows x-ray exposure for Al at 30 keV. The normalized total energy flux is divided into three parts: the transmission fraction, the absorption fraction, and the scattering-out fraction. The upper curve describes the energy deposition process, $\{1 - [1 - \exp(-\sigma_{\text{tot}}(E) x \rho)] \sigma_{\text{abs}}(E) / \sigma_{\text{tot}}(E)\}$, just the reverse of the absorption curves; the lower curve describes the attenuation process, where energy decays by the total cross section $[\exp(-\sigma_{\text{tot}}(E) x \rho)]$. Since a part of the scattering energy is also absorbed in $\sigma_{\text{incohabs}}(E)$, the difference between the two curves indicates the scattering out or scattering loss of the energy flux, not the total scattered flux. A fraction of this scattering loss of energy flux would be reabsorbed as secondary radiation.

Figure 8. X-Ray Attenuation in Al
(at 30 keV)

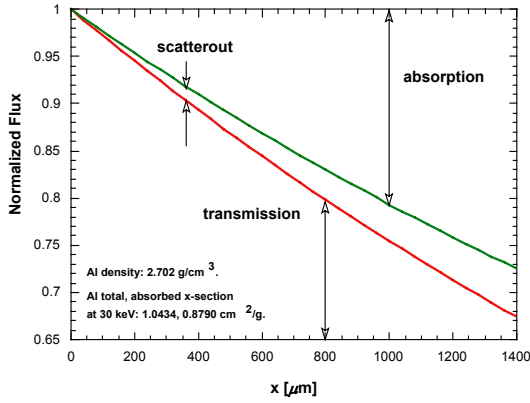
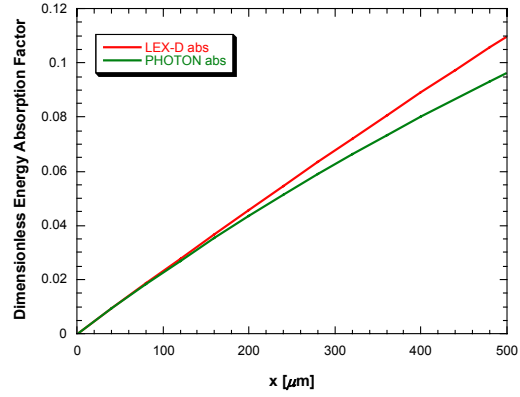


Figure 9. Dimensionless Absorption Factor
Modeled by LEX-D and PHOTON



For example, it would contribute partially to backscattering for a material layer at its bottom surface and would be reabsorbed by the layer (see the section Two-Layer Scattering Model and Example Calculations). Figure 9 is a plot of the LEX-D and PHOTON normalized energy absorption factors for the parameters in Figure 8. The two models use different expressions for the energy absorption factor. PHOTON uses $\{[1 - \exp(-\sigma_{\text{abs}}(E) x \rho)] \exp(-\sigma_{\text{tot}}(E) x \rho)\}$, while LEX-D uses $\{[1 - \exp(-\sigma_{\text{tot}}(E) x \rho)] \sigma_{\text{abs}}(E) / \sigma_{\text{tot}}(E)\}$. (Figure 9 shows generic absorption without empirical parameters for self-absorption and fluorescence). At 500 μm , the difference for Al at 30 keV would be about 12%, although for an 80- μm Al filter the difference is only about 2%. Conceptually, the PHOTON expression is not appropriate, since $[1 - \exp(-\sigma_{\text{tot}}(E) x \rho)]$ is a factor of transmission loss in a layer with thickness x , and $\sigma_{\text{abs}}(E) / \sigma_{\text{tot}}(E)$ is the fraction being absorbed. The derivative of both of them with respect to x —the slope of both curves—is this difference. The physical meaning of the derivative of the absorbed energy is the dose per unit incident flux $(1 / I_0) dI/dx$ at x , where I_0 is the incident intensity and

$$(d/dx) \{ [1 - \exp(-\sigma_{\text{tot}}(E) x \rho)] \sigma_{\text{abs}}(E) / \sigma_{\text{tot}}(E) \} = \exp(-\sigma_{\text{tot}}(E) x \rho) \rho \sigma_{\text{abs}}(E)$$

for LEX-D,

$$(d/dx) \{ [1 - \exp(-\sigma_{\text{abs}}(E) x \rho)] \exp(-\sigma_{\text{tot}}(E) x \rho) \} = \exp(-\sigma_{\text{tot}}(E) x \rho) \rho \sigma_{\text{abs}}(E)$$

$$- \{ [1 - \exp(-\sigma_{\text{abs}}(E) x \rho)] \exp(-\sigma_{\text{tot}}(E) x \rho) \sigma_{\text{tot}}(E) \rho \} \quad \text{for PHOTON.}$$

The correct dose expression is $I_0 \exp(-\sigma_{\text{tot}}(E) x \rho) \rho \sigma_{\text{abs}}(E)$, so the expression used in LEX-D is appropriate, since $I_0 \exp(-\sigma_{\text{tot}}(E) x \rho)$ is the energy flux transmitted at depth x , and $\rho \sigma_{\text{abs}}(E)$ times that is the absorbed dose rate. The extra term in the PHOTON expression is ambiguous, which contributes to the slope difference between the two curves.

ENERGY LOSS IN COMPTON SCATTERING

In scattering, according to quantum theory,^[1] if a photon with frequency ν , energy E , and momentum $p = (h \nu)/c$ is propagating along x direction (where c is the speed of light and h is Planck's constant), assuming the photon meets a free electron at the coordinate origin, the collision between photon and electron causes the electron to gain kinetic energy, e_k . This kinetic energy can be expressed as

$$e_k = mc^2 - m_0c^2 = m_0c^2 [(1 - \beta^2)^{-1/2} - 1]$$

where m is the mass of the electron after collision, m_0 is the rest mass of the electron, and $\beta = v/c$, where v is the velocity of the recoil electron. The momentum of the electron is $P_e = mv$. After collision, the photon will propagate in a new direction θ with a decreased energy E' , decreased frequency ν' , or increased wavelength λ' . The momentum of the photon becomes $p' = h\nu'/c$. At the same time, the recoil electron is ejected in a direction ϕ . Then $\nu' < \nu$, $\lambda' > \lambda$, and $E' < E$ for a non-zero θ . Since $E = E' + e_k$, the frequency change is

$$\nu = \nu' + m_0c^2 [(1 - \beta^2)^{-1/2} - 1] h^{-1}$$

Momentum balance gives two component equations, $p' \cos \theta + P_e \cos \phi = p$ and $p' \sin \theta + P_e \sin \phi = 0$. They can be rewritten as one expression after ϕ is eliminated:

$$(\nu - \nu')^2 + 2 \nu \nu' (1 - \cos \theta) = m_0^2 c^4 \beta^2 (1 - \beta^2)^{-1} h^{-2}$$

Therefore, $\nu' = \nu'(\theta)$, which means the frequency and hence the energy of the postcollision photon depends solely on the scattering angle θ . Combining energy and momentum balances, and eliminating β , the wavelength change $\Delta\lambda$ and the photon energy loss ΔE will be

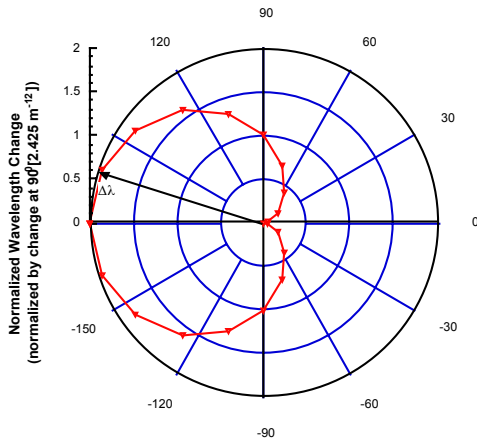
$$\Delta\lambda = \lambda' - \lambda = c/\nu' - c/\nu = (1 - \cos \theta) h (m_0c)^{-1}$$

$$\Delta E = E - E' = 1 - [1 + (1 - \cos \theta) E (m_0c^2)^{-1}]^{-1}$$

If $E \ll (m_0c^2)$, for energies very much lower than the rest mass energy of the electron, (m_0c^2) , there is almost no energy loss, and at $\Delta E/E \ll 1$, the scattering approaches coherent scattering. It can be seen that $\Delta\lambda = \Delta\lambda(\theta)$ and $E' = E(\theta, \lambda)$. $\Delta\lambda$ does not depend on λ ; it depends only on scattering angle θ , while E' is a function of both θ and λ . At $\theta = 0$, $\lambda' = \lambda$

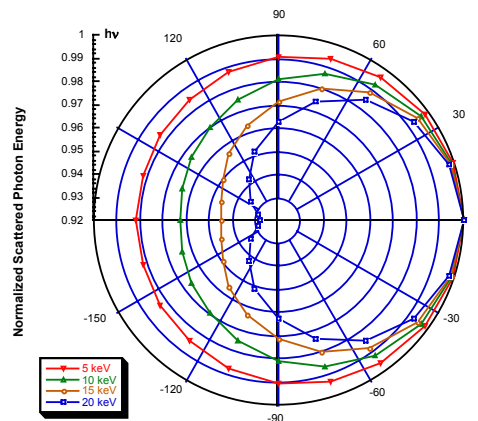
, and $E' = E$, no scattering occurs; at $\theta = \pi$, maximum energy loss occurs. From $\theta = 0$ to $\theta = \pi/2$, it is frontscattering, and from $\theta = \pi/2$ to $\theta = \pi$, it is backscattering. The value of $\Delta\lambda$ is about 2.4 m^{-12} for $\theta = \pi/2$; $\Delta\lambda_{max}$ is about 4.8 m^{-12} for $\theta = \pi$. Here $h(m_0c)^{-1} = 2.4 \text{ m}^{-12}$ is the Compton wavelength of the electron. Figure 10 shows wavelength gain (normalized by its value at $\pi/2$) as a function of scattering angle. Figure 11 shows the scattered photon energy change E'/E (normalized by original energy) with scattering angle θ for original photon energies at 5, 10, 15, and 20 keV. The maximum photon energy change $\Delta E/E$ increases from 2% for 5 keV to 7.3% for 20 keV and can be extended to

Figure 10. Wavelength Change After Compton Scattering (independent of frequency)



13.6% for 40 keV at $\theta = \pi$. Such a loss cannot be ignored.

Figure 11. Compton Photon Energy vs. Scattering Angle



The above equation for wavelength change is based on the assumption that the photon interacts with a stationary free electron, not an electron in motion and being bound energetically to the atom. To accommodate this assumption, Bloch introduced a correction term that is proportional to the square of the wavelength. The coefficient of the term depends on numbers of electrons and shell energy level for up to three shells. The correction term (Blohkin^[26]) is not included here, since it is important only for long wavelengths. For shorter wavelengths, which are of interest here, it is a second-order effect and can be disregarded.

In reality, the scattering angle value is not totally random (see Figure 15). As a first approximation, assuming uniform scattering over all possible angles, we defined an average scattering angle for a range of angles as the angle at which the scattering energy is equal to the integrated average scattering energy over the same range of angles. Let θ_1 , θ_2 , and θ_3 denote the average total scattering, average frontscattering, and average backscattering angle, respectively, and E'_1 , E'_2 , and E'_3 denote the average total scattered, average frontscattered, and average backscattered energy, respectively. Letting e'_1 , e'_2 , and e'_3 be the dimensionless values of E'_1 , E'_2 , and E'_3 , respectively, by rest mass energy (m_0c^2), then

$$\begin{aligned}
 e'_1(\lambda) &= (1/\pi) \int_0^\pi [1 + e(\lambda)(1 - \cos \theta)]^{-1} d\theta \\
 &= (1 + 2e(\lambda))^{-1/2} \\
 e'_2(\lambda) &= (2/\pi) \int_0^{\pi/2} [1 + e(\lambda)(1 - \cos \theta)]^{-1} d\theta \\
 &= (1 + 2e(\lambda))^{-1/2} (4/\pi) \arctan[(1 + 2e(\lambda))^{1/2}] \\
 e'_3(\lambda) &= (2/\pi) \int_{\pi/2}^\pi [1 + e(\lambda)(1 - \cos \theta)]^{-1} d\theta \\
 &= 2(1 + 2e(\lambda))^{-1/2} \{1 - (2/\pi) \arctan[(1 + 2e(\lambda))^{1/2}]\}
 \end{aligned}$$

To find the average scattering angles θ_1 , θ_2 , and θ_3 , we need to solve the equation

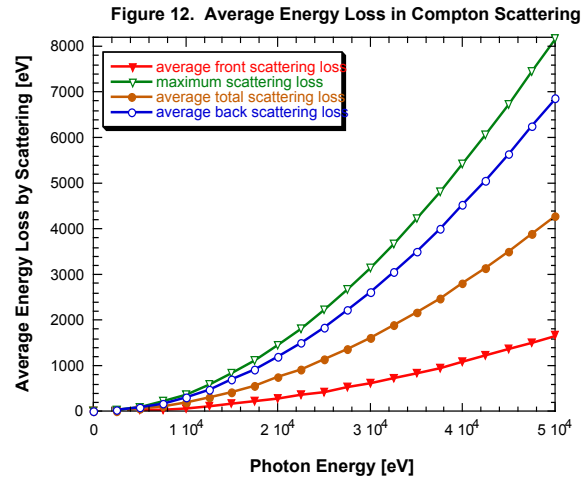
$$e'(\theta, \lambda) = [1 + e(\lambda)(1 - \cos \theta)]^{-1}$$

for $e'(\theta_1, \lambda) = e'_1$, $e'(\theta_2, \lambda) = e'_2$, and $e'(\theta_3, \lambda) = e'_3$, respectively. For the first equation, $e'(\pi/2, \lambda) = (1 + e(\lambda))^{-1}$. We can see that $(e'_1(\lambda))^2$ and $(e'(\pi/2, \lambda))^2$ are identical if one neglects the second-order term $(e(\lambda))^2$. Doing so can be justified, since the value of rest mass energy (m_0c^2) used to normalize is relatively large—about 511 keV, well beyond the

photon energy range of LIGA interest. Therefore, the average total scattering angle for the LIGA photon energy region is $\theta_1 = 0.5\pi$ (the average over $\theta = 0$ to π), which is actually sidescattering, or the maximum frontscattering angle. A comparison of calculations for many $e(\lambda)$ functions indicates that θ_2 is about 0.3π (the average over $\theta = 0$ to $\pi/2$) and θ_3 is about 0.7π (the average over $\theta = \pi/2$ to π). Both the average frontscattering angle and the average backscattering angle are closer to $\pi/2$ than to π . In other words, they are on average close to sidescattering. Therefore, using the average scattering angle to estimate the scattering effect could overestimate the frontscattering effect and could underestimate the backscattering effect for any single scattering event. Here the average scattering angles are used only to obtain an initial estimate. By definition, we know that E_1 , E_2 , and E_3 satisfy $(1/2)(E_2 + E_3) = E_1$. The average scattering angles have a similar relation $(1/2)(\theta_1 + \theta_2) = \theta_3$, because the energy loss function $E'(\theta, \lambda)$ is roughly antisymmetric about $\theta = \pi/2$.

To estimate the average energy loss in Compton scattering, we evaluate the average photon energy loss over these three average scattering angles. Figure 12 shows curves of losses for average front-, back-, and total scattering and for maximum scattering, which in a

rigorous sense $\square\square$ backscattering at $\theta = \pi$. We can see that the maximum energy loss at 50 keV could reach 8 keV at 16% for backscattering at $\theta = \pi$, while the average backscattering loss at 50 keV could reach 6.8 keV at 13.7%. The average frontscattering loss is only 1.7 keV at 3.4%. The average total scattering loss at 50 keV is 4.2 keV, about 8.4%, which certainly underestimates the backscattering losses if backscattering occurs.



A very important equation in Compton scattering, used by almost all databases, is the Klein-Nishina equation. Klein and Nishina derived the Compton collision cross section from Dirac's quantum mechanics for interaction between a photon and a free electron early in 1929.^[27] The differential collision cross section per unit solid angle for unpolarized radiation is a function of scattering angle θ and dimensionless photon energy $e = E / (m_0c^2)$, expressed as:

$$(d\sigma/d\omega) = (r_e^2/2)(1 + \cos^2\theta) \{1 + e^2(1 - \cos\theta)^2 / [f_{\alpha\theta}(1 + \cos^2\theta)]\} / f_{\alpha\theta}^2$$

$$f_{\alpha\theta} = 1 + e(1 - \cos \theta)$$

where r_e is the radius of an electron (2.8179×10^{-13} cm) and ω is solid angle; $(1 + \cos^2 \theta)/2$ is the polarization factor of the scattering ray. In the case of a polarized radiation ray, $\cos^2 \theta$ would be a factor for incident electric vector lying in the incident plane, and 1 would be a factor for incident electric vector perpendicular to the incident plane. In the case of a nonpolarized ray, the average of the two is used. Integrating the above equation over all solid angles results in the Compton cross section for an electron. The equation multiplied by the Compton energy loss fraction ($h\nu'/h\nu$) and then integrated over all solid angles results in the Compton scattering-out cross section. The difference between these two integrals becomes the Compton scattering energy deposition cross section.

Figure 13 shows $(d\sigma/d\omega)$ curves for several values of e (0, 0.02, 0.05, 0.1, 0.15, 0.19). For 100 keV, which is the upper limit of the photon energy in this case, $e = 0.19569$. As e approaches zero, Compton scattering approaches Thompson scattering (coherent scattering). Therefore, the curve for $e = 0$ is symmetrical about $\pi/2$. In this case, frontscattering and backscattering are equally likely. It can be seen for non-zero e that the cross section decreases if the scattering angle θ increases, and it decreases more rapidly for higher e . This means that frontscattering has a greater probability than backscattering for high photon energy; backscattering has a greater probability for low photon energy than for high photon energy.

Figure 14 shows the ratio of the backscattering collision cross section ($\theta = \pi, 5/6\pi, 2/3\pi, 1/2\pi$) to the frontscattering collision cross section ($\theta = 0$) for a power spectrum. It can be seen clearly that the backscattering probability decreases with increasing photon energy: it decreases by 30%, 36%, 52%, and 58% as photon energy increases from zero to 50 keV for the above four scattering angles, respectively. It is also interesting to see the coherent scattering probabilities for backscattering from this figure. As $E = 0$, when Compton scattering approaches coherent scattering, the backscattering probabilities are reduced about 12%, 37%, and 50% for backscattering angles at $\theta = 5/6\pi, 2/3\pi,$ and $1/2\pi$, compared with the probability at an angle of $\theta = \pi$. Here $E = 0$ should not be understood as actual zero photon energy, but instead as any very low photon energy for which coherent scattering occurs.

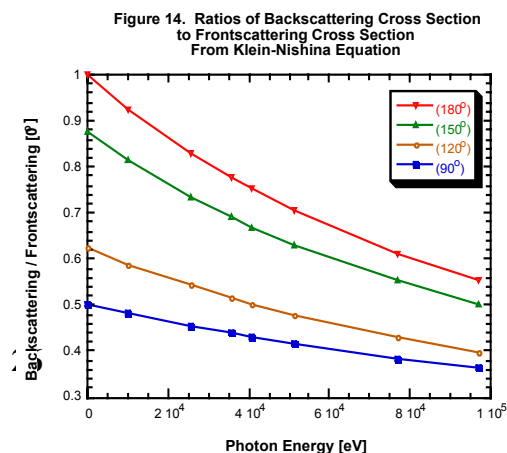
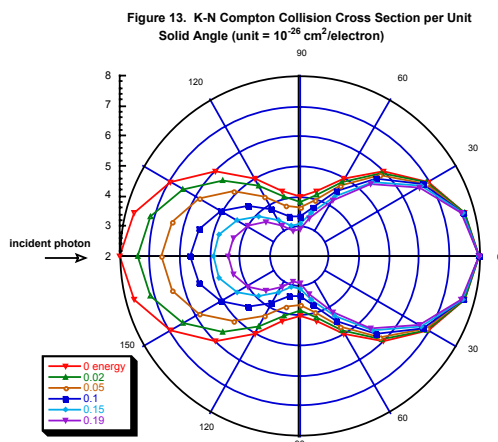
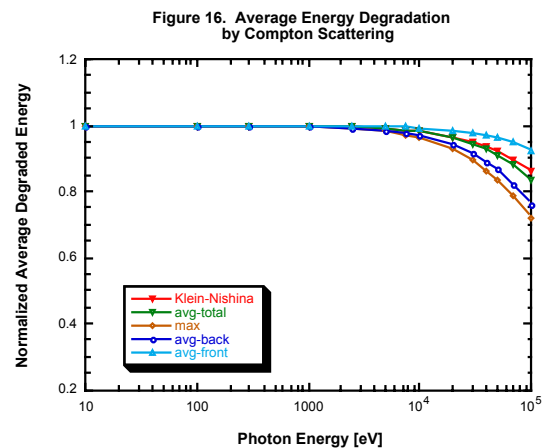
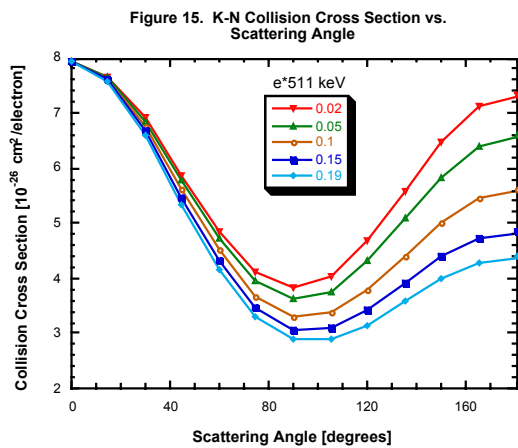


Figure 15 stretches the angle to an x - y plot. If the areas under the curves are normalized, these cross-section curves for different photon energies are actually scattering probability density functions. Figure 16 is a comparison of average energy degradation in Compton scattering calculated on the basis of a degradation value from the Klein-Nishina equation and our average energy loss results.^[24] The differences based on our average total scattering energy loss ($\theta_1 = 90^\circ$) for a scattered 50-, 70-, and 100-keV photon are about 0.88%, 1.5%, and 2.56%, respectively. The agreement is very good. The average frontscattering curve, the average backscattering curve, and the maximum scattering curve re located above or below, accordingly.



The correction for binding electronic effect (bound electron) was included in an incoherent scattering function by Hubbell^[25] in 1969. As an example, the factor is 1.55 for K-shell electrons of Au for $\theta = 180^\circ$ at $e = 662$ keV. This correction can be ignored for lighter elements, however, since for lower photon energy, where binding effect is important, photoelectric effects dominate the total cross section over the scattering effects. For higher photon energy, where photoelectric effects contribute only a small part of the total, binding effects become negligible compared with the energy of the incident photon. For C, for example, the photoelectric effect is about 99.94% of the total cross section at 1 keV, and it decreases to 11.58% at 38.7 keV.

TWO-LAYER SCATTERING MODEL AND EXAMPLE CALCULATIONS

The scattering model sums the contributions of scattering from the resist itself and from its adjacent layer, assuming the layer above the resist is generally a filter and the layer below is a substrate. In backscattering, a fraction of the x-ray flux reaches the resist-substrate interface and then scatters back into the resist, and another fraction of the x-ray flux reaches all the way to the bottom of the substrate and then scatters back and is transmitted backward to the interface. Similarly, in frontscattering, in addition to the contribution of the resist itself, a fraction of the x-ray flux frontscattered from the filter in front of the resist reaches the top surface of the resist and then is transmitted to the interface. Here the contributions from above the filter and below the substrate are ignored, since they are higher-order contributions compared with those of the filter and substrate.

The scattered-out energy flux excluding the absorption part of the scattering energy is

$$Q_{\text{scatout}}(x) = \int_0^{\infty} I_{\text{scatout}}(E, x) dE$$

$$I_{\text{scatout}}(E, x) = I(E', x_1) \{1 - \exp[-\sigma_{\text{tot}}(E')(x - x_1) \rho]\} (\sigma_{\text{tot}}(E') - \sigma_{\text{abs}}(E')) / \sigma_{\text{tot}}(E')$$

$$E' = E[1 - E(m_0c^2)^{-1}(1 - \cos \theta)]^{-1}$$

where E' is the original photon energy before scattering loss corresponding to post-scattering, E, x is the depth at which the scattering is estimated, $Q_{\text{scatout}}(x)$ is total scattered-out energy flux, $I_{\text{scatout}}(E, x)$ is the scattered-out energy flux spectrum, and $I(E', x_1)$ is the incident energy flux at the top surface of the current layer (here the current layer would be the resist, and x_1 is at its top surface), θ is the scattering angle, and (m_0c^2) is the electron rest mass energy. It is recognized that the factor $(\sigma_{\text{tot}}(E') - \sigma_{\text{abs}}(E')) / \sigma_{\text{tot}}(E')$ is the fractional scattered loss or scattered-out flux. Therefore, the process of calculation for backscattering would be to choose a backscattering angle θ first and then, for each photon energy E in the spectrum, calculate the corresponding pre-scattering photon energy E' , estimate all material cross sections involved at E' , and calculate and combine the contributions from both the resist and the substrate. Note that integration here is carried over post-scattering photon energy E instead of pre-scattering energy E' . The total backscattering energy flux at the interface is hence

$$Q_{\text{back}}(x_1 + d^{\text{resist}}) = Q_{\text{backscatout}}^{\text{resist}}(x_1 + d^{\text{resist}}) + Q_{\text{back}}^{\text{substrate}}(x_1 + d^{\text{resist}})$$

$$\begin{aligned}
& Q_{\text{back}}^{\text{substrate}}(x_1 + d^{\text{resist}}) \\
&= \int_0^{\infty} I^{\text{substrate}}(E', x_1 + d^{\text{resist}}) [1 - \exp(-\sigma_{\text{tot}}^{\text{substrate}}(E') d^{\text{substrate}} \rho^{\text{substrate}})] \\
&\times [(\sigma_{\text{tot}}^{\text{substrate}}(E') - \sigma_{\text{abs}}^{\text{substrate}}(E')) / \sigma_{\text{tot}}^{\text{substrate}}(E')] \exp(-\sigma_{\text{tot}}^{\text{substrate}}(E) d^{\text{substrate}} \rho^{\text{substrate}}) dE
\end{aligned}$$

where d is the thickness. The last exponential factor in $Q_{\text{back}}^{\text{substrate}}(x)$ in the first expression is the backward transmission fraction of the substrate backscattered energy flux. Note that here the last factor of transmission (the second exponential function) uses postscattering photon energy E , while the remainder of the integrand describes scattering out and uses pre-scattering photon energy E' . For backscattering, the scattering angle implicitly used here must be from 90° to 180° . In the example, an average scattering angle $\theta_3 = 126^\circ$ (0.7π) and maximum scattering angle $\theta = 180^\circ$ are used. The resulting total backscattering dose rate is

$$\begin{aligned}
D_{\text{back}}(x_1 + d^{\text{resist}}) &= \int_0^{\infty} I^{\text{resist}}(E', x_1) [1 - \exp(-\sigma_{\text{tot}}^{\text{resist}}(E') d^{\text{resist}} \rho^{\text{resist}})] \\
&\times [(\sigma_{\text{tot}}^{\text{resist}}(E') - \sigma_{\text{abs}}^{\text{resist}}(E')) / \sigma_{\text{tot}}^{\text{resist}}(E')] \sigma_{\text{abs}}^{\text{resist}}(E) \rho^{\text{resist}} dE \\
&+ \int_0^{\infty} I^{\text{substrate}}(E', x_1 + d^{\text{resist}}) [1 - \exp(-\sigma_{\text{tot}}^{\text{substrate}}(E') d^{\text{substrate}} \rho^{\text{substrate}})] \\
&\times [(\sigma_{\text{tot}}^{\text{substrate}}(E') - \sigma_{\text{abs}}^{\text{substrate}}(E')) / \sigma_{\text{tot}}^{\text{substrate}}(E')] \\
&\times \exp(-\sigma_{\text{tot}}^{\text{substrate}}(E) d^{\text{substrate}} \rho^{\text{substrate}}) \sigma_{\text{abs}}^{\text{resist}}(E) \rho^{\text{resist}} dE
\end{aligned}$$

The two terms at the right of the dose expression are the contributions from the resist itself and from the substrate, respectively. Note again that the last transmission factor and the last absorption factor in the second term (the last line of the equation) use postscattering photon energy E , while all other functions in the integrand describing scattering out use pre-scattering photon energy E' . Similarly, for the total frontscattering energy flux and dose rate at the interface

$$\begin{aligned}
Q_{\text{front}}(x_1 + d^{\text{resist}}) &= Q_{\text{frontscatout}}^{\text{resist}}(x_1 + d^{\text{resist}}) + Q_{\text{front}}^{\text{filter}}(x_1 + d^{\text{resist}}) \\
Q_{\text{front}}^{\text{filter}}(x_1 + d^{\text{resist}}) &= \int_0^{\infty} I^{\text{filter}}(E', x_1 - d^{\text{filter}}) [1 - \exp(-\sigma_{\text{tot}}^{\text{filter}}(E') d^{\text{filter}} \rho^{\text{filter}})]
\end{aligned}$$

$$\begin{aligned}
& \times [(\sigma_{\text{tot}}^{\text{filter}}(E') - \sigma_{\text{abs}}^{\text{filter}}(E')) / \sigma_{\text{tot}}^{\text{filter}}(E')] \exp(-\sigma_{\text{tot}}^{\text{resist}}(E)d^{\text{resist}}\rho^{\text{resist}})dE \\
D_{\text{front}}(x_1 + d^{\text{resist}}) = & \int_0^{\infty} I^{\text{resist}}(E', x_1 [1 - \exp(-\sigma_{\text{tot}}^{\text{resist}}(E')d^{\text{resist}}\rho^{\text{resist}})]) \\
& \times [(\sigma_{\text{tot}}^{\text{resist}}(E') - \sigma_{\text{abs}}^{\text{resist}}(E')) / \sigma_{\text{tot}}^{\text{resist}}(E')] \sigma_{\text{abs}}^{\text{resist}}(E)\rho^{\text{resist}} dE \\
& + \int_0^{\infty} I^{\text{filter}}(E', x_1 - d^{\text{filter}}) [1 - \exp(-\sigma_{\text{tot}}^{\text{filter}}(E')d^{\text{filter}}\rho^{\text{filter}})] \\
& \times [(\sigma_{\text{tot}}^{\text{filter}}(E') - \sigma_{\text{abs}}^{\text{filter}}(E')) / \sigma_{\text{tot}}^{\text{filter}}(E')] \\
& \times \exp(-\sigma_{\text{tot}}^{\text{resist}}(E)d^{\text{resist}}\rho^{\text{resist}})\sigma_{\text{abs}}^{\text{resist}}(E)\rho^{\text{resist}} dE
\end{aligned}$$

The last exponential factor in $Q_{\text{front}}^{\text{filter}}(x)$ is the forward transmission fraction of the filter frontscattered energy flux, so the transmission is occurring in the resist instead of the filter; that is why the parameters used here are for the resist. For frontscattering, the scattering angle must be from 0° to 90° . In the example, $\theta_2 = 54^\circ$ (0.3π) and $\theta_1 = 90^\circ$ are used.

The model applies to an NSLS standard filter set and a PMMA resist with various substrate materials. Incident x rays from the NSLS synchrotron with a scan length of 7.6 cm pass through a Be window of 500 μm , an Al filter of 50 μm , and an air layer of 800,000 μm to a PMMA resist of 990 μm and a substrate of 100 μm . A variety of substrate materials are calculated, including Be, Si, Cu, Au, Al, Ni, and Ti. The results, presented as values integrated over the entire spectrum, are shown in the table. The first column denotes the material of the substrate, as well as flags for average front-, average total, average back-, and maximum scattering, respectively. The second column is the input power flux and top-surface dose for the PMMA resist. The third column is the total scattering power flux [W/cm^2] and the scattered bottom-surface dose rate [W/cm^3] at the bottom surface of the PMMA resist. The fourth column is the secondary-scattering power flux and the secondary-scattering surface dose (same units as previous columns) at the interface contributed from the substrate for backscattering and from the filter for frontscattering. The fifth and the sixth column are the ratio values of the third column to the second column and of the fourth column to the second column, respectively.

The data show that the average total and average frontscattering power fluxes at the interface are the sum of the contributions from the PMMA itself and from the air above it. The contribution from the air layer is close to half the total. In this case, an 80-cm space of air made a noticeable contribution to frontscattering. The percentages of the average total and frontscattering power fluxes are about 4%. The average backscattering power fluxes

and surface dose rate at the interface are the sum of the contributions from the PMMA itself and from the substrate. The percentages of the average backscattering and maximum backscattering fluxes and surface dose rates are approximately 2.04–2.3%, while the percentage contribution from the substrate, which is a secondary effect, is one order smaller, or within 0.23%. The average backscattering and the maximum scattering power fluxes or surface dose rate percentages for the different substrate materials are all of the same order of magnitude, 2.04–2.28%. The Be, Si, Al, and Ti substrates contribute about one order of magnitude more than Cu, Au, and Ni. In other words, substrates with lower atomic numbers scatter back more. This confirms that Compton scattering is important for low- Z materials, since a light atom has looser electrons (smaller binding energies) in its outer shell than a heavy atom has. Even with this difference, the average scattering power fluxes and surface dose rates remain at the same levels. Thus, the contribution from the PMMA itself dominates backscattering. The total and secondary frontscattering effect is larger than the total and secondary backscattering effect. Secondary frontscattering is at least one order of magnitude larger than secondary backscattering. The main reason for this is that the substrate receives a smaller incoming energy flux because of absorption by filters and the resist.

Scattering Results for NSLS Standard Filter Set + Resist + Substrate

Substrate/Flag	powin [W/cm2]	totscat [W/cm2]	sndscat [W/cm2]	tscat/powin	snds/powin
	dostop [W/cm3]	scatdos [W/cm3]	snddos [W/cm3]	scados/dostop	sndos/dostop
1-avg front	0.664542	2.60E-02	1.21E-02	3.92E-02	1.82E-02
$\theta_2 = 0.3 \pi$	1.19361				
2-avg total	0.664542	2.50E-02	1.16E-02	3.76E-02	1.74E-02
$\theta_1 = 0.5 \pi$	1.19361				
Be					
3-avg back	0.664542	1.45E-02	1.50E-03	2.18E-02	2.25E-03
$\theta_3 = 0.7 \pi$	1.19361	2.69E-02	2.51E-03	2.25E-02	2.10E-03
4-max back	0.664542	1.41E-02	1.46E-03	2.13E-02	2.20E-03
$\theta_4 = 1.0 \pi$	1.19361	2.72E-02	2.53E-03	2.28E-02	2.12E-03
Si					
3	0.664542	1.44E-02	1.42E-03	2.17E-02	2.13E-03
	1.19361	2.59E-02	1.52E-03	2.17E-02	1.28E-03
4	0.664542	1.40E-02	1.37E-03	2.11E-02	2.05E-03
	1.19361	2.62E-02	1.52E-03	2.19E-02	1.28E-03
Cu					
3	0.664542	1.32E-02	2.34E-04	1.99E-02	3.52E-04
	1.19361	2.44E-02	3.97E-05	2.05E-02	3.33E-05
4	0.664542	1.29E-02	2.12E-04	1.94E-02	3.18E-04
	1.19361	2.47E-02	3.62E-05	2.07E-02	3.03E-05
Au					
3	0.664542	1.30E-02	2.98E-05	1.95E-02	4.48E-05
	1.19361	2.44E-02	1.06E-06	2.04E-02	8.88E-07
4	0.664542	1.27E-02	2.80E-05	1.90E-02	4.21E-05
	1.19361	2.47E-02	9.78E-07	2.07E-02	8.20E-07
Al					
3	0.664542	1.46E-02	1.64E-03	2.20E-02	2.47E-03
	1.19361	2.62E-02	1.83E-03	2.20E-02	1.53E-03
4	0.664542	1.43E-02	1.59E-03	2.14E-02	2.39E-03
	1.19361	2.65E-02	1.83E-03	2.22E-02	1.53E-03
Ni					
3	0.664542	1.32E-02	2.65E-04	1.99E-02	3.98E-04
	1.19361	2.44E-02	4.14E-05	2.05E-02	3.47E-05
4	0.664542	1.29E-02	2.40E-04	1.94E-02	3.60E-04
	1.19361	2.47E-02	3.86E-05	2.07E-02	3.23E-05
Ti					
3	0.664542	1.37E-02	7.33E-04	2.06E-02	1.10E-03
	1.19361	2.47E-02	3.03E-04	2.07E-02	2.54E-04
4	0.664542	1.34E-02	6.87E-04	2.01E-02	1.03E-03
	1.19361	2.50E-02	2.95E-04	2.09E-02	2.47E-04
NSLS source	Be 500 μm	Al 50 μm	Air 800000 μm	PMMA 990 μm	substrate 100 μm

The values of these scattering dose rates are about $0.025\text{--}0.027\text{ W/cm}^3$. The exposure time must be included to show the dose values in J/cm^3 . In these examples, if approximately 8 kJ/cm^3 is a required dose at the PMMA top surface and the exposure time is 2 hours, then the extra dose at the bottom surface of the shadow region (masked region) of the PMMA would be $180\text{--}195\text{ J/cm}^3$. If the exposure time is longer, the scattering dose will be larger.

The maximum backscattering amount is not necessarily larger than the average backscattering amount. The “max” means the maximum photon energy loss during scattering. As photon energy shifts to the left on the axis (to a smaller value), the power spectrum at the new photon energy may be larger or smaller than the old value, depending on which side of the peak power flux it is situated. The “max” scattering amount could be either larger or smaller than the “average” scattering amount. There are several examples in the table where the scattering power flux or dose rate for average backscattering is greater

than the maximum backscattering. A detailed backscattering energy distribution over the spectrum is shown in Figures 17 and 18 for a Si substrate. Figure 17 is a backscattering power spectrum, and Figure 18 is a backscattering dose rate spectrum. The total backscattering curves remain about two orders of magnitude smaller than the incident power spectrum for the entire spectrum. The secondary backscattering contribution grows beyond 10 keV , which is about one order smaller than the total backscattering. This confirms the dominant contribution of the resist backscattering.

Figure 17. Average Backscattered Power Fluxes for NLSL Example

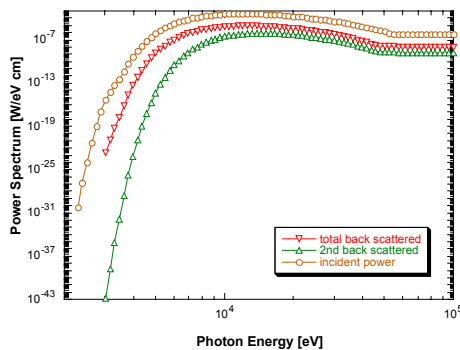
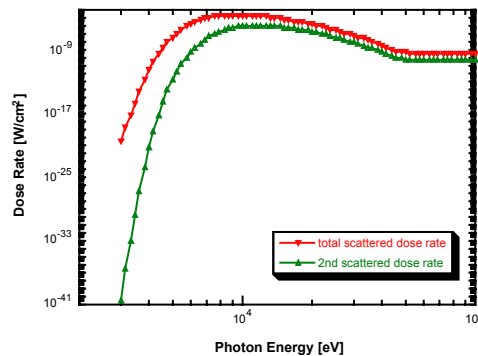


Figure 18. Average Backscattered Dose Rate for NLSL Example



The above calculated absorbed dose values (less than 200 J/cm^3) are not very significant. The reason is that the incoming power spectrum at the resist is not strong enough to produce significant Compton scattering effects. The peak of the incoming power spectrum is at the wavelength at which the photon has an energy more or less around 10 keV . At this photon energy range, Compton scattering is not important.

There are many factors that could possibly be the direct or indirect causes of undercutting or overcutting: the three-dimensional feature shape, feature size, and aspect ratio of the designed pattern of the resist; the probability of backscattering; and the polarization of the x ray, which the model does not address. A one-dimensional model cannot fully explain three-dimensional corner undercutting. It can serve only as an average scattering model to provide the scattering basics and some physical insights. The unwanted dose distribution on the bottom or top surface of the resist shadow region, which is two-dimensional, would be valuable for LIGA exposure. Because of the limited capacity of even modern computers, researchers have so far performed Monte Carlo simulations either with low input power (too few photons) or with photons of only a monochromatic wave. Research with a three-dimensional simulation is still in the early stage.

Unlike coherent scattering, incoherent scattering does not have the same probability for frontscattering and backscattering. The assumption of uniform scattering over all possible angles for Compton scattering may either underestimate or overestimate the backscattering effect. The introduction of probability of scattering based on the Klein-Nishina collision cross section versus scattering angles (see Figure13) is a good approach. Because the probability for frontscattering is generally larger than that of backscattering (Figure13), it appears that this approach always overestimates backscattering and underestimates frontscattering, from the standpoint of scattering probability. Such an approach is safe at this point, since backscattering is the issue of most concern here.

Calculated two-dimensional examples^[28] of the scattering x rays that arrive at the resist masked region from the resist open region, under the standard filter set of the NSLS synchrotron source, indicate a competition between two factors: attenuation over distance, and the Klein-Nishina probability of the scattering angle. The resulting two-dimensional absorbed dose profile at the vertical cross section of the resist shows that the maximum absorbed doses occur at the upper and lower corners of the masked region right at the open-masked boundary, which would seem to contribute to undercutting. Fortunately, the values of those maximum doses are well below 100 J/cm^3 .

None of the approaches considers polarization. Since an x ray is an electromagnetic wave, it can be polarized. X rays coming from a synchrotron light source are polarized in the electron orbit plane. Incident radiation is linearly polarized: a large component of the velocity of the emitted photoelectron is parallel to the direction of the electric field of the incident radiation. For polarized radiation, the Compton scattering cross section depends on the direction of the electric vector of the incident radiation. In this case, the Klein-Nishina differential collision cross section will become

$$(d\sigma/d\omega) = (r_e^2/2)(\nu'/\nu)^2[(\nu'/\nu) + (\nu/\nu') - 2 \sin^2 \theta \cos^2 \phi]$$

where θ is the scattering angle and ϕ is the polarization angle, which is the angle between the scattering plane and the plane of the incident photon and its electric vector. Note that it would increase the cross section except for $\theta = 0^\circ$ and 180° exactly. At $\phi = 0^\circ$, the cross section has its minimum value; at $\phi = 90^\circ$, it has its maximum value; at $\phi = 45^\circ$, it has the average value of the two, which is chosen as the value for the nonpolarized case, as in the previous Klein-Nishina equation. Therefore, the average value could be either underestimated or overestimated for a collision cross section.

Not only scattering x rays but also fluorescence x rays (or characteristic x-ray spectral lines), photoelectrons, and Auger electrons (see appendix) may contribute to undercutting or sidewall dissolution of LIGA features. Part 2 of this report addresses the effects of fluorescence x rays in detail. For example, Ti, a mid-Z element, has a K absorption edge (K-shell binding energy) at about 5 keV; its cross section jumps across the edge. For an incident photon with energy just greater than that absorption edge energy, the photon energy is absorbed by the Ti atom completely, and the atom becomes excited. During the relaxation process, the atom may emit a Ti K fluorescence x-ray line, which has a unique wavelength of 2.497 angstrom, less than the Ti K-shell binding energy. It may be directed backward or sideward, since fluorescence x rays do not have a preferred direction. Examples in Part 2 show that the extra energy from the fluorescence x rays emitted at the resist-substrate interface can penetrate the resist shadow region and significantly increase doses. Future studies are needed on the subject of undercutting caused by photoelectrons and Auger electrons.

Nonuniform temperature causing heat conduction is another possible source of resist damage. The thermal conductivity of the resist is usually much lower than that of metal. The absorption of x rays by the resist results in nonuniform heating of the material within gaps and columns of the microstructure after exposure, especially for structures with small features and a large aspect ratio. Further investigation in this direction is also needed. To avoid a distortion of the microstructure due to thermal expansion of the resist, a good thermal conductor such as a metal may be selected as the substrate or inserted as a thin layer between the resist and the substrate. A mid-high-Z material such as Ti may be a good choice. However, the mid-high-Z materials are the ones that would emit fluorescence x rays and photoelectrons that could reduce the adhesion between the resist and the substrate if the surface dose of the material is large enough.^[9,11,12] In this case, a preabsorber could be used to limit the fluorescence x rays the material emits.^[9]

CONCLUSION OF PART 1

X-ray scattering/backscattering and fluorescence x-ray emissions during LIGA exposure are addressed separately in Part 1 and Part 2, respectively.

Compton (incoherent) scattering is dominant in the photon energy range of LIGA exposure. Calculation examples from our two-layer scattering model show that for a variety of substrate materials, the total backscattering x-ray dose at the resist-substrate interface comprises two parts. The major part is the primary x-ray radiation energy, which penetrates the resist and scatters at the interface. The second part is the radiation energy that penetrates the substrate, scatters backward at the bottom surface of the substrate, and reaches the interface. It is at least one or two orders smaller than the primary x-ray radiation, depending on the substrate material. The scattering effect is stronger for low- Z materials and is weaker for high- Z materials because the outer-shell electrons of a light atom are easier to excite than those of a heavy atom. However, the differences in scattering doses among many substrate materials (Be, Al, Si, Ti, Ni, Cu, Au) are small compared with the total scattering dose. The average dose rate is in a range from $2.47 \times 10^{-2} \text{ W/cm}^3$ for an Au substrate to $2.72 \times 10^{-2} \text{ W/cm}^3$ for a Be substrate, under an NSLS synchrotron source and an NSLS standard filter set. Whether these dose rates will cause damage to the PMMA resist when x-ray energy penetrates the resist shadow region depends on the exposure time. For a dose of 8 kJ/cm^3 at the top surface of the resist and an exposure time of 2 hours, the total dose will be about $180\text{--}195 \text{ J/cm}^3$ in the shadow region. This dose will not significantly affect development.

In summary, the above absorbed doses due to scattering are not significant. The reason is that the incoming power spectrum at the resist is not strong enough to produce significant Compton scattering effects under most LIGA exposure conditions. In the examples, the incoming power flux at the resist is 0.665 W/cm^2 and the peak of the power spectrum is $3.97 \times 10^{-4} \text{ W/cm}^2$ per eV, at which point the photon has an energy around 12 keV. At this photon energy, Compton scattering is not important. Further, since the NSLS spectrum is harder than those of SSRL and ALS, scattering alone cannot cause undercutting or significant loss of tolerances of the resists for any of the sources used by Sandia.

REFERENCES

1. M. X. Tan, M. A. Bankert, S. K. Griffiths, A. Ting, D. R. Boehme, S. Wilson, and L. M. Balser, PMMA Development Studies Using Various Synchrotron Sources and Exposure Conditions, *Proceedings of the SPIE Symposium on Micromachining and Microfabrication*, Santa Clara, California, September 20–22, *Materials and Device Characterization in Micromachining* **3512**, 1998.
2. J. M. Hruby, M. A. Bankert, T. E. Bennett, D. R. Boehme, W. D. Bonivert, S. K. Griffiths, J. T. Hachaman, J. S. Krafcik, Jr., A. M. Morales, and A. Ting, LIGA Prototyping at Sandia National Laboratories, Third International Conference on High Aspect Ratio Microstructure Technology (HARMST 1999), Kisarazu Chiba, Japan, June 13–15, 1999.
3. A. M. Morales, J. M. Hruby, T. Bennett, M. Bankert, D. R. Boehme, W. D. Bonivert, J. T. Hachman, S. K. Griffiths, R. H. Nilson, A. Ting, L. Domeier, and P. Keifer, LIGA Micromachining at Sandia National Laboratories, 4th International Conference on the Commercialization of Microsystems, Dortmund, Germany, July 10, 1999.
4. J. M. Hruby, A. Morales, L. Domeier, W. D. Bonivert, D. R. Boehme, M. A. Bankert, J. T. Hachmann, S. Leith, S. K. Griffiths, and A. Ting, LIGA: Metals, Plastics and Ceramics, *Proceedings of the SPIE Symposium on Micromachining and Microfabrication*, Santa Clara, California, September 20–22, *Micromachining and Microfabrication Process Technology* **3874** (2), 1999.
5. D. R. Boehme, J. M. Hruby, W. D. Bonivert, M. A. Bankert, J. T. Hachman, A. M. Morales, D. M. Skala, S. K. Griffiths, A. Ting, T. E. Bennett, J. S. Krafcik, Jr., S. D. Leith, and D. Chinn, LIGA R&D and Prototyping, Semicon West 1999, San Francisco, California, July 14, 1999.
6. S. K. Griffiths, J. M. Hruby, and A. Ting, Optimum Doses and Mask Thickness for Synchrotron Exposure of PMMA Resists, *Proceedings of the SPIE Symposium on Design, Test and Microfabrication of MEM/MOEMS*, Paris, France, March 30–April 1, 1999.
7. S. K. Griffiths, A. Ting, and J. M. Hruby, The Influence of Mask Substrate Thickness on Exposure and Development Times for the LIGA Process, *J. Microsystem Technologies* **6** (3), 99–102, February 2000.

8. S. K. Griffiths, J. M. Hruby, and A. Ting, The Influence of Feature Sidewall Tolerance on Minimum Absorber Thickness for LIGA X-Ray Masks, *J. Micromech. Microeng.* **9** (4), 353–361, December 1999 (featured article).
9. F. J. Pantenburg and J. Mohr, Influence of Secondary Effects on the Structure Quality in Deep X-Ray Lithography, *Nuclear Instruments and Methods in Physics Research B* **97**, 551–556, 1995.
10. H. Zumaque, G.A. Kohring, and J. Hormes, Simulational Studies of Energy Deposition and Secondary Processes in Deep X-Ray Lithography, *J. Micromech. Microeng.* **7**, 79–88, 1997.
11. G. Feiertag, W. Ehrfeld, H. Lehr, A. Schmidt, and M. Schmidt, Accuracy of Structure Transfer in Deep X-Ray Lithography, *Microelectronic Engineering* **35**, 557–560, 1997.
12. G. Feiertag, W. Ehrfeld, H. Lehr, A. Schmidt, and M. Schmidt, Calculation and Experimental Determination of the Structure Transfer Accuracy in Deep X-Ray Lithography, *J. Micromech. Microeng.* **7**, 323–331, 1997.
13. K. Murata, Theoretical Studies of the Electron Scattering Effect on Developed Pattern Profiles in X-Ray Lithography, *J. Appl. Phys.* **57** (2), January 1985.
14. A. Schmidt, A. Clifton, W. Ehrfeld, G. Feiertag, H. Lehr, and M. Schmidt, Investigation of the Adhesive Strength of PMMA Structures on Substrates Obtained by Deep X-Ray Lithography, *Microelectronic Engineering* **30**, 215–218, 1996.
15. Center for X-Ray Lithography, University of Wisconsin at Madison, The CXrL: Toolset Users Guide, Version 1.0, 1993.
16. A. Ting, S. Griffiths, LEX-D Version 3.1, Sandia LIGA group, May 1998.
17. D. Chapman, N. Gmur, N. Lazarz, and W. Thomlinson, PHOTON: A Program for Synchrotron Radiation Dose Calculations, National Synchrotron Light Source, Brookhaven National Laboratory, Upton, New York, 1988.
18. D. Chapman, PHOTON: A User's Manual, National Synchrotron Light Source, Brookhaven National Laboratory, January 1988.

19. Center of X-Ray Optics (CXRO), Lawrence Berkeley National Laboratory, The X-Ray Attenuation Length of a Solid, from X-Ray Interaction with Matter, 1993.
20. B. L. Henke, E. M. Gullikson, and J. C. Davis, Low-Energy X-Ray Interaction Coefficients: Photoabsorption, Scattering, and Reflection at $E = 30\text{--}30,000$ eV, $Z = 1\text{--}92$, Atomic Data and Nuclear Data Tables, Lawrence Berkeley National Laboratory, July 1993.
21. D. E. Cullen, M. H. Chen, J. H. Hubbel, S. T. Perkins, E. F. Plechaty, J. A. Rathkopf, and J. H. Scofield, Tables and Graphs of Photon-Interaction Cross Sections from 10 eV to 100 GeV Derived from the LLNL Evaluated Photon Data Library (EPDL), UCRL-50400, Vol. 6, LLNL, October 1989.
22. F. Biggs and R. Lighthill, Analytical Approximations for X-Ray Cross Sections III, SAND87-0070, Sandia National Laboratories Report, August 1988.
23. F. Biggs and R. Lighthill, Analytical Approximations for Total and Energy Absorption Cross Sections for Photon-Atom Scattering, SC-RR-72 0685, Sandia National Laboratories Report, December 1972.
24. R. K. Cole, Jr., BUCKL: A Program for Rapid Calculation of X-Ray Deposition, SC-RR-69-855, Sandia National Laboratories Report, July 1970.
25. J. H. Hubbel and S. M. Seltzer, Tables of X-Ray Mass Attenuation Coefficients and Mass Energy-Absorption Coefficients 1 keV to 20 MeV for Elements $Z = 1$ to 92 and 48 Additional Substances of Dosimetric Interest, NISTIR 5632, National Institute of Standards and Technology (NIST), 1996.
26. M. A. Blokhin, *Physics of X-Rays* (Translation Series), Oak Ridge, Tennessee, 1961.
27. O. Klein and Y. Nishina, *Z. Physik* **52**, 853, 1929.
28. A. Ting, Distribution of Scattering X-Rays in Resist Shadow Region from Resist Open Region, Sandia internal memo, June 2000.

APPENDIX: BASIC INTERACTIONS BETWEEN PHOTONS AND ATOMS

Inside an atom, electronic energy levels, or shells, are situated such that the binding energy is largest for K-shell electrons because they are the closest to the positively charged nucleus and progressively lower for the shells farther from the nucleus (the L through Q shells). The outermost shell electrons are free, or valence, electrons and the inner shell electrons are bound, or orbit, electrons.

Five types of basic interactions may occur between the photons and atoms along the beam path: photoelectric interaction, coherent scattering, incoherent (Compton) scattering, pair production, and triplet production. A brief description of how these interactions contribute to x-ray attenuation follows.

Photoelectric Cross Section

Photoelectric interaction occurs when the energy of an incident photon is greater than the binding energy of the electrons in one of the inner shells. The atom absorbs all of the photon's energy, and the photon disappears. Then the atom is in an excited state because of the excess energy, and it ejects an electron as a photoelectron from that shell, leaving a vacancy and becoming ionized positively. An electron from an outer shell fills the vacancy, accompanied by either the emission of a characteristic x-ray photon (fluorescence x ray) or the ejection of an Auger electron. New vacancies in the outer shells will be filled in the same way until the atom loses its excited state and returns to its normal, or ground, state.

From the standpoint of conservation of energy, the energy of the incident photon equals the binding energy of the shell plus the kinetic energy of the photoelectron. The energy of the fluorescence x ray is the energy difference between the two interacting shells. The total energy of a series of characteristic photons in a single photoelectric interaction plus the local energy deposition equals the binding energy of the initial inner shell.

There are two kinds of secondary radiation in this interaction: the photoelectric effect (some researchers consider this primary radiation) and fluorescence. In the low-keV photon energy range, photoelectric effect is the dominant process. It contributes most of the local energy deposition. Energy is re-emitted as fluorescence x rays, which are quite penetrating for transferring photons. This energy is deposited at some distance from the point where the photon interacted with the atom. Fluorescence may be important for high-Z materials and decreases by roughly an order of magnitude for each successive shell (see Part 2).

Coherent Scattering Cross Section

At very low energy, an x-ray photon interacts with a relatively bound outer orbit electron and sets the electron into vibration. This produces an electromagnetic wave with the same energy as the incident photon but with a different direction. The incident photon has been scattered without undergoing any change in wavelength, frequency, or energy. This is coherent scattering, or elastic scattering, and is related to Rayleigh scattering. It is described by classical Thompson scattering theory. It may be important for high- Z materials, since they consist of heavy atoms. It approaches zero as photon energy approaches zero.

Incoherent Scattering Cross Section

Incoherent scattering is also called Compton scattering or inelastic scattering. An incident photon with sufficient energy interacts with a loosely bound outer-shell electron, with the result that the photon proceeds in a different direction with less energy, longer wavelength, and lower frequency—and accompanied by an emitted electron. The electron is called a Compton, or recoil, electron. The process causes ionization of atoms. The energy of the incident photon is transferred to the recoil electron, and the scattered photon has less energy than the incident photon.

Compton scattering dominates in the intermediate (high-keV to low-MeV) photon energy range, where photon energy may be significantly greater than binding energy. This is particularly important for low- Z materials, since they consist of light atoms. At the low energy range, Compton scattering approaches coherent scattering as photon energy approaches zero.

Pair and Triplet Production

When a very high energy (beyond a few MeV) photon interacts with the field of an entire atom, the photon disappears and an electron-positron pair is created. When a photon interacts with the field of an electron, not only is a pair created but also an electron is ejected from the atom, leaving an ionized atom. In terms of energy conservation, the incident photon energy must be greater than the rest mass energy of the pair or triplet for the event to occur. A single rest mass energy value is m_0c^2 , or about 511 keV. The rest mass energy of a pair would be as high as 1.022 MeV.

DISTRIBUTION:

1 MS 0329 E. J. Garcia, 2614

1 MS 0329 A. D. Oliver, 2614

1 MS 0503 D. W. Plummer, 2330

1 MS 0603 T. R. Christenson, 1743

1 MS 9001 M. E. John, 8000
Attn: R. C. Wayne, 2800, MS 9005
J. Vitko, 8100, MS 9004
W. J. McLean, 8300, MS 9054
P. N. Smith, 8500, MS 9002
K. E. Washington, 8900, MS 9003

1 MS 9007 D. R. Henson, 8400

1 MS 9042 G. H. Evans, 8728

1 MS 9042 S. K. Griffiths, 8728

1 MS 9042 M. F. Horstemeyer, 8728

1 MS 9042 W. G. Houf, 8728

1 MS 9042 R. S. Larson, 8728

1 MS 9042 C. D. Moen, 8728

1 MS 9042 R. H. Nilson, 8728

10 MS 9042 A. Ting, 8728

1 MS 9401 M. A. Bankert, 8729

1 MS 9401 J. M. Hruby, 8702

1 MS 9401 J. T. Hachman, 8729

1 MS 9401 C. Henderson, 8729

1 MS 9401 R. P. Janek, 8729

1 MS.9401 A. M. Morales, 8729

1	MS 9401	R. Shediac, 8729
1	MS 9401	D. M. Skala, 8729
1	MS 9405	R. H. Stulen, 8700 Attn: R. Q. Hwang, 8721, MS 9161 W. R. Even, 8722, MS 9402 J. C. F. Wang, 8723, MS 9403 W. A. Kawahara, 8725, MS 9042 E. P. Chen, 8726, MS 9161 J. L. Handrock, 8727, MS 9042
1	MS 9405:	K. L. Wilson, 8724
1	MS 9409	H. A. Bender, 8730
1	MS 9671	D. A. Chinn, 8729
3	MS 9017	Central Technical Files, 8945-1
1	MS 0899	Technical Library, 9616
1	MS 9021	Classification Office, 8511/Technical Libarary, MS 0899, 9616
1	MS 9021	Classification Office, 8511 for DOE/OSTI